Politecnico di Milano
Facoltà di Ingegneria
Corso di laurea in Ingegneria Aeronautica
Dipartimento di Scienze e Tecnologie Aerospaziali

Blowing Snow in Aeronautical Application: a new Statistical Model by means of Bayesian Approach

Relatore: Prof. Alberto Guardone
Correlatore: Dott. Giulio Gori

Tesi di Laurea di:
Alessio Raimondi Matr. 900291

Anno Accademico 2019-2020

Contents

Chapter 1

Introduction

1.1 The *Snow Problem* for in-flight ice accretion

Why studying the snow is relevant for in-flight ice accretion. What PoliMIce (PoliDrop) needs from this study: $c_D(Re, param)$ formula and a rule to choose the parameters.

1.2 State of Art

1.2.1 Non-spherical particles

Introduction to available models: nothing generated precisely for snow application but many models present for arbitrary-shaped particles. Generally the models are validated using particles with various known shapes, but not with snowflakes.

Generic model formula: $c_D = c_D(d_v, Re, \underline{\Phi})$

Models and Experiments examples

Explanation of figures like 1.1 and 1.2.

1.2.2 Snow experiments

Introduction to available snow experiments. For aerodynamic purposes the most relevant type of measure is the ground experiment conducted with some kind of disdrometer. It gives a measure the particle dimension (often its mean diameter) and a measure of its terminal velocity.

1.3 Blowing vs Falling regime

Problem with the difference between the regime of the simulations and the regime of the experiments. Our assumption: the model we chose is able to transfer the information about the shape of the particle from the falling to the blowing regime.

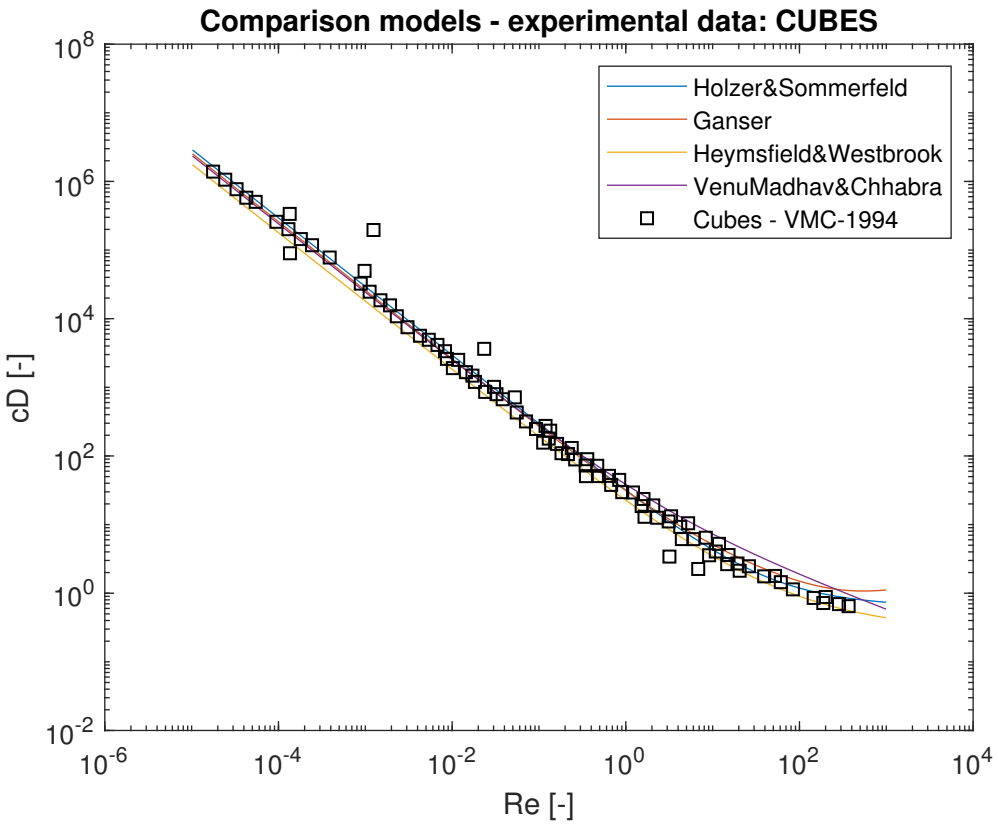

Figure 1.1

1.4 Research Question

Goal of the thesis: The question proposed in Section 1.1 will be answered by:

1. Choose a suitable model for the description of the snow c_D
2. Use that model to infer the statistical distribution of the shape parameters of a given *cloud* in the *falling regime*
3. Transfer this information to the *blowing regime* by implementing the same model with the same parameter distribution in PoliDrop

1.5 Structure of the thesis

Chapter description

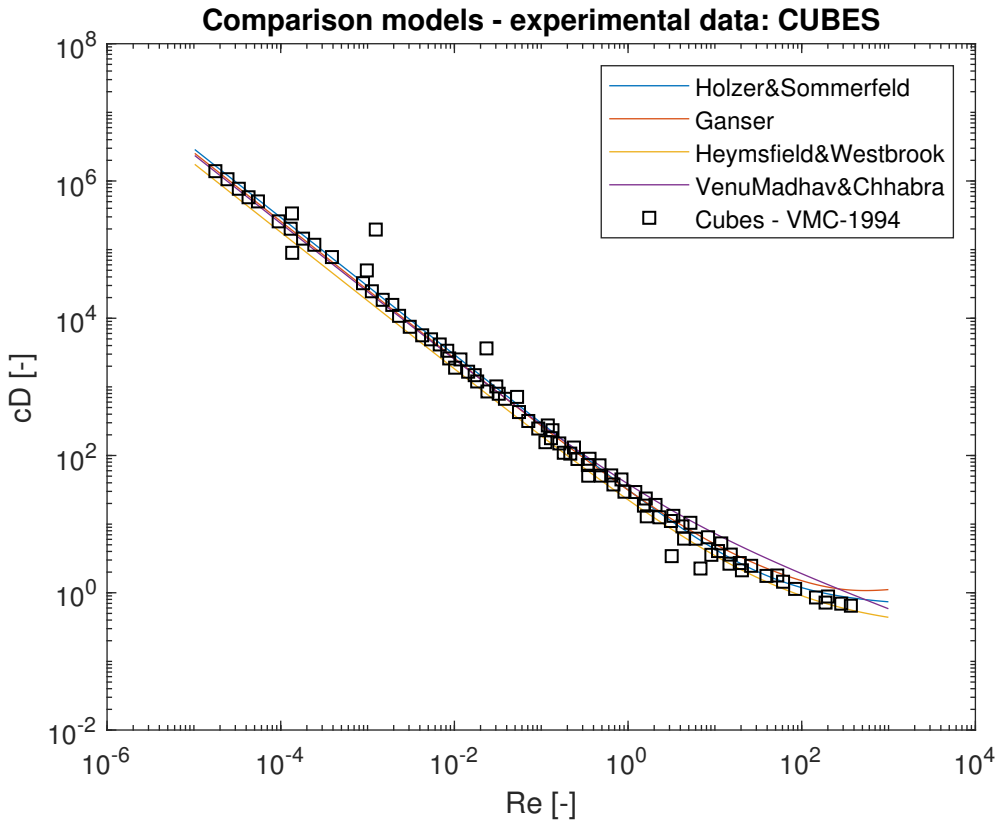
Comparison models - experimental data: CUBES
Holzer&Sommerfeld
Ganser
Heymsfield&Westbrook
VenuMadhav&Chhabra
Cubes - VMC-1994
cD [-]
Re [-]
10^8
10^6
10^4
10^2
10^0
10^-2
10^-6
10^-4
10^-2
10^0
10^2
10^4

Figure 1.2

Chapter 2

Review of Falling-Snow Models

This chapter will explore the model of the snowflake as an arbitrary-shaped particle in free fall. The governing equation will be described and, with that, the need of a model for the drag coefficient in order to close the problem. Consequently, the theoretical framework behind a general drag coefficient model will be explained and some of the available models in literature will be reviewed and compared.

As discussed in Section 1.4, we are not interested in all the dynamics behind the free fall of the snowflakes, but only in their terminal velocity, that is the maximum velocity attainable by an object as it falls by effect of the gravity field. It is obtained, in the case of snow, when the sum of the drag (F_D) and the buoyancy force (F_B) balances the weight of the particle (W). Under the assumption that the effects of aerodynamic forces and moments, on direction other than the falling one, are negligible, the governing equation reads:

$$\underbrace{\frac{1}{2}\rho v_t^2 S_\perp c_D(Re, \text{model}, \text{parameters})}_{F_D} = \underbrace{\frac{\pi}{6} d_\text{v}^3 \rho_\text{p} g}_{W} - \underbrace{\frac{\pi}{6} d_\text{v}^3 \rho g}_{F_B} \tag{2.1}$$

which, after some simplification, can be written as:

$$v_\text{t}^2 c_D(Re(v_\text{t}, d_\text{v}), \text{model}, \text{parameters}) = \frac{\pi}{3} \frac{\rho_{\text{p}(d_\text{v})} - \rho}{\rho} \frac{d_\text{v}^3}{S_\perp} g \tag{2.2}$$

where rho is the density of air and g is the magnitude of the gravity field. These two parameters are constants.

The characteristic dimension of the particle (d_v) is generally taken as the *volume diameter*, that is the diameter of the sphere that has the same volume of the particle, namely:

$$d_\text{v} = \sqrt[3]{\frac{6V_\text{p}}{\pi}} \tag{2.3}$$

This dimension is an independent variable of the problem, in fact it is one of the values provided by the experimental data.

The Reynolds number of the particle is based on the relative velocity of the fluid w.r.t. the particle:

$$Re = \frac{u\ d_\text{v}}{\nu} \qquad \text{with:} \qquad u := ||\underline{u}_f - \underline{u}_p|| \tag{2.4}$$

The reference surface $S_\perp$ is taken as the area of the particle projected to a plane perpendicular to the velocity vector and can be retrieved from the model if it accounts for the orientation of the particle; it is taken as πd_v^2 otherwise. The specialization of this value for each model will be presented with the model itself.

For the calculation of the particle density ρ_p, an empirical formula found by Brandes [**Brandes-2008**] is used:

$$\rho_{\mathrm{p}(d_\mathrm{v})} = 0.178\ d_\mathrm{v}^{-0.922} \tag{2.5}$$

where the density of snow is measured in kg/m^3 and the diameter is measured in m. This is not a widely diffused formula, a further improvement of the thesis could consist in inferring also this parameter.

In order to close the problem and solve numerically the Equation 2.2, a model for the drag coefficient needs to be specified. It will contain a dependency on the Reynolds number and on some additional parameter, which number and definition will vary based on the chosen model.

In 1999 Chhabra et al. published a review article on non-spherical particles [**ChhabraEtAl-1999**]. They evaluated a selection of the most used correlations methods using experimental results culled from 19 independent studies, consisting of 1900 data points with wide ranges of physical and kinematics conditions. The performances of the methods were evaluated by calculating the mean and maximum error between the experimental value and the value predicted by the models. The analysis has been carried on both with respect to a single shape category (sphere, cube, cylinder and so on) and also considering the overall data set. The best method appeared to be that of Ganser [**Ganser-1993**], which will be discussed in the following section. Yet, a more significant contribution of this article was the definition of a new standard for a non-spherical particle model, stating that a good correlation formula must account for information on 2 main aspects: *shape* of the particle and *orientation* of the particle.

The parameter mainly used to describe the shape of the particle is the *sphericity*, which is the ratio between the surface area of the volume-equivalent sphere and the area of the actual particle:

$$\Phi = \frac{\pi\ d_\mathrm{v}^2}{A_\mathrm{p}} \tag{2.6}$$

This is a common element between various models. The choice of the parameter that describes the particle orientation is more ample, thus each one of those parameters will be presented in relation with the linked model.

In the following sections the Ganser model, alongside with a more recent one, will be reviewed and compared on the basis of the available literature.

Info on the other discarded models.

2.1 The Ganser Model

The Ganser model [**Ganser-1993**] comes from empirical correlations of the general drag formula by Haider and Levenspiel [**HaiderLevenspiel-1989**]:

$$c_D = \frac{24}{Re}(1 + ARe^B) + \frac{C}{1 + \frac{D}{Re}} \tag{2.7}$$

It relies on the notion that a good c_D formula must involve a dependence on at least two shape descriptors. Using similarity arguments and dimensional analysis, Ganser showed that knowledge of the Stokes' shape factor (K_1) and of the Newton's shape factor (K_2) is sufficient for accurate prediction of the drag over a large range of Reynolds number. Geometric shape descriptors such as sphericity are used to model K_1 and K_2 and not c_D, directly.

The basic assumption in this paper is that every isolated particle experiences a Stokes' regime where the drag is proportional to velocity and a Newton's regime where the drag is proportional to the square of velocity.

In addition, it is possible to extract shape and orientation factors from the behaviour of the particle in the Stokes's and Newton's regimes with dimensional analysis. Then, the way a particle behaves in these two regimes can be used to predict the drag for a large range of Reynolds numbers.

The general definition for the Stokes' shape factor reads:

$$K_1 = \left(\frac{1}{3}\frac{d_\mathrm{n}}{d_\mathrm{v}} + \frac{2}{3}\Phi^{-\frac{1}{2}}\right)^{-1} - 2.25\frac{d_\mathrm{v}}{D_\mathrm{tube}} \tag{2.8}$$

where the importance of both the shape and the orientation of the particle in the viscous regime ($Re \ll 1$) is measured by the *sphericity* (Φ) and the ratio between the *normal diameter* (diameter of the sphere with the equivalent projected area) and the *volume diameter* ($d_\mathrm{n}/d_\mathrm{v}$), as already claimed by Leith [**Leith-1987**] (who first introduced the Stokes' shape factor). Physically, values of $d_\mathrm{n}/d_\mathrm{v}$ greater than 1 correspond to a particle with the axis parallel to the direction of motion bigger than the other one as prolate spheroids and cylinders. Particles with $d_\mathrm{n}/d_\mathrm{v} < 1$ are, instead, more similar to oblate spheroids and disks. Since we will consider only snowflakes falling in an open environment, the second term is negligible, as $D_\mathrm{tube} \to \infty$.

Thompson and Clark [**ThompsonClark-1991**] defined the Newton's shape factor as the ratio between the drag coefficient of a particle of a certain shape and the drag coefficient of a sphere, both at Reynolds number of 10 000, following the argument that, at high Reynolds (Newton's regime), the c_D is approximately constant. From this observation, Ganser derived the following formula for the Newton's shape factor:

$$K_2 = 10^{1.8148(-log(\Phi))^{0.5743}} \tag{2.9}$$

The final version of the model is function of the *generalized* Reynolds number (ReK_1K_2) and reads:

$$c_D = K_2\left(\frac{24}{ReK_1K_2}(1 + 0.1118(ReK_1K_2)^{0.6567}) + \frac{0.4305}{1 + \frac{3305}{ReK_1K_2}}\right) \tag{2.10}$$

The specialization of the reference surface $S_\perp$ that is needed in Equation 2.2 is given by:

$$S_\perp = \pi d_\mathrm{n}^2 = \pi\left(\frac{d_\mathrm{n}}{d_\mathrm{v}}\right)^2 d_\mathrm{v}^2 \tag{2.11}$$

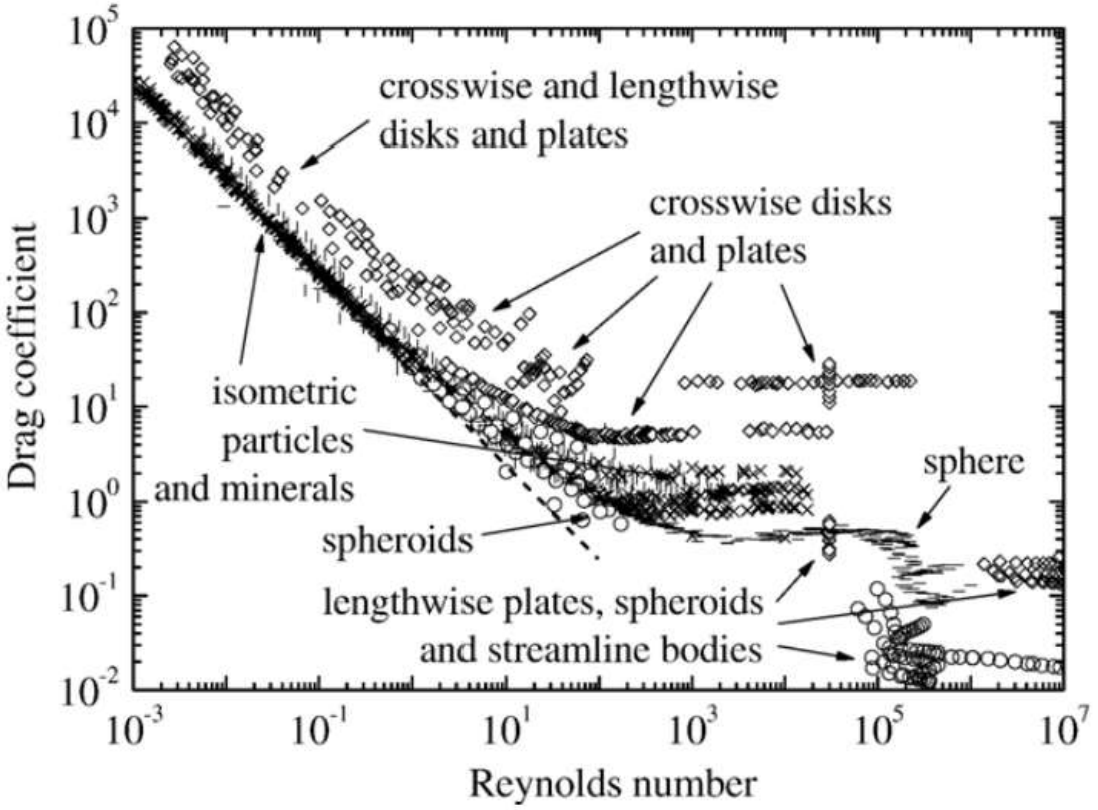

Figure 2.1: Drag coefficient of different shaped particles as function of the Reynolds number. Data from the literature review of Holtzer and Sommerfeld. [**HoltzerSommerfeld-2008**] Legend: - - Stokes, — Sphere, ◇ Disks and plates, × Isometric bodies, | Minerals, ○ Spheroids and streamline bodies.

2.2 The Hölzer and Sommerfeld Model

The model by Höltzer and Sommerfeld [**HoltzerSommerfeld-2008**] is, in effect, an interpolation of previous models coming from an extensive literature review. The coefficients of their final formula are tuned on a collection of over two thousand experimental data. The c_D values used are summarized in Figure 2.1, featuring spheres, disk and plates, lengthwise spheroids and streamline bodies, isometric particles such as cubes, tetrahedrons and octahedrons, and irregularly shaped particles such as minerals.

Similarly to Ganser, they used different models for the Stokes' and the Newton's regime. The Stokes' region is characterized by an inverse proportionality between the drag coefficient and the Reynolds number. The formula used is the one suggested by Leith [**Leith-1987**]:

$$c_D = \frac{8}{Re}\frac{1}{\sqrt{\Phi_\perp}} + \frac{16}{Re}\frac{1}{\Phi} \tag{2.12}$$

where the particle orientation is measured by the crosswise sphericity ($\Phi_\perp$), which is defined in Equation 2.13 as the ratio between the cross-sectional area of the volume-equivalent sphere w.r.t. the cross-sectional area of the actual particle projected on

a plane perpendicular to the velocity vector ($A_{\mathrm{p},\perp}$).

$$\Phi_\perp = \frac{\frac{\pi}{4}\, d_\mathrm{v}^2}{A_{\mathrm{p},\perp}} \tag{2.13}$$

Again, to give a physical interpretation of this shape descriptor, values of $\Phi_\perp$ lesser than 1 correspond to a particle with the axis parallel to the direction of motion bigger than the other one as prolate spheroids and cylinders. On the contrary, particles with $\Phi_\perp > 1$ are more similar to oblate spheroids and disks. The first term in Equation 2.12 stands for the pressure or form drag, associated with the size of the projected cross-sectional area, while the second term represents the friction drag, associated with the size of the surface area. Correlation with experimental data showed that the use of the lengthwise sphericity ($\Phi_{/\!/}$) instead of $\Phi_\perp$ in Equation 2.12 leads to a better approximation of the c_D in the Stokes region. The lengthwise sphericity is defined in Equation 2.14 as the ratio between the cross-sectional area of the volume-equivalent sphere and the difference between half the surface area (A_p) and the mean longitudinal (i.e. parallel to the direction of relative flow) projected cross-sectional area of the actual particle ($\bar{A}_{\mathrm{p},/\!/}$). Since $A_{\mathrm{p},/\!/}$ depends on the angle of view, an arithmetic average over an entire revolution is used.

$$\Phi_{/\!/} = \frac{\frac{\pi}{4}\, d_\mathrm{v}^2}{\Delta A} \qquad \text{with:} \qquad \Delta A = \frac{A_\mathrm{p}}{2} - \bar{A}_{\mathrm{p},/\!/} \tag{2.14}$$

For the Newton's regime two different models are used. The first one represents the friction drag of lengthwise particles (small cross-sectional area). The mathematical model describing this phenomenon is, according to Blasius' theory:

$$c_D = 1.327 \cdot 2 \left(\frac{8}{9}\right)^{\frac{1}{4}} \pi^{\frac{1}{4}} \left(\frac{\text{depth}}{\text{length}}\right)^{\frac{1}{4}} \frac{1}{\Phi^{\frac{3}{4}}} \frac{1}{\sqrt{Re}} \tag{2.15}$$

which, for square plates, reduces to:

$$c_D = 3.43/(\Phi^{\frac{3}{4}}\sqrt{Re}) \tag{2.16}$$

and this simplified version will be used.

The second model derives from the study of Tran-Cong et al [**TranCongEtAl-2004**] and represents the behaviour of isometric and cross-wise oriented bodies. The c_D of such particles in the Newton's regime is almost solely determined by form drag, in particular it is approximately proportional to the reciprocal of crosswise sphericity. Merging this study with the literature by Ganser and Leith, Höltzer and Sommerfeld proposed the following formula for isometric and crosswise oriented particles at high Reynolds number:

$$c_D = 0.4210^{0.4(-\log\Phi)^{0.2}} \frac{1}{\Phi_\perp} \tag{2.17}$$

The correlation formula for the c_D over the entire range of Re results from the addition of Equations 2.12, 2.16 and 2.17:

$$c_D = \frac{8}{Re}\frac{1}{\sqrt{\Phi_{/\!/}}} + \frac{16}{Re}\frac{1}{\sqrt{\Phi}} + \frac{3}{\sqrt{Re}}\frac{1}{\Phi^{\frac{3}{4}}} + 0.4210^{0.4(-\log\Phi)^{0.2}} \frac{1}{\Phi_\perp} \tag{2.18}$$

In the same paper, they also derived a simplified model of similar performance, in terms of accuracy w.r.t. all the available data, depending on two parameters only, namely Φ and $\Phi_\perp$, which reads:

$$c_D = \frac{8}{Re}\frac{1}{\sqrt{\Phi_\perp}} + \frac{16}{Re}\frac{1}{\sqrt{\Phi}} + \frac{3}{\sqrt{Re}}\frac{1}{\Phi^{\frac{3}{4}}} + 0.4210^{0.4(-\log\Phi)^{0.2}}\frac{1}{\Phi_\perp} \tag{2.19}$$

During this thesis we will take advantage of the simplified model, since it reduces the number of unknowns.

The specialization of the reference surface $S_\perp$ that is needed in Equation 2.2 is given by:

$$S_\perp \approx A_{\mathrm{p},\perp} = \frac{\pi}{4\Phi} \tag{2.20}$$

2.3 Model comparison

Both the models presented so far have the characteristics to properly describe an arbitrary-shaped particle. Referring to the comparison done by Hölzer and Sommerfeld [**HoltzerSommerfeld-2008**], the Ganser formula works better with isometric particle, having a mean relative deviation of 6.46%, over the one of 10.9% of Equation 2.19. These statistics come from the comparison of the c_D expected by the model w.r.t. the one found in the literature, considering 655 experimental data. Using the same type of comparison they found that their model has an edge on the calculation of the c_D of disk and plates (386 values), with a mean deviation of 16.8% over the $1.8 \cdot 10^3$% of Ganser's. Also, the overall performance of the second model appears to be better: 14.4% compared to 348% over all the 2061 values considered.

Although it seems that the model by Hölzer and Sommerfeld is the better one, it must be considered that the data used for the comparison are the same data that have been used to develop the model. A comparison with more recent experiments and perhaps different geometries would be required to properly compare the two formulae. Unfortunately, such data are not present in the literature yet and an experimental campaign for this purpose is unfeasible.

The path we chose is to carry out a sensitivity study of the two models w.r.t. their free parameters (the shape descriptors), comparing them with the curves provided by Brandes [**BrandesIkedEtAl-2008**]. These relations have on the abscissa the volume diameter of the particle and on the ordinate the mean terminal velocity of the snowflakes measured in their experimental campaigns.

For a more in-depth discussion on the calculation of the terminal velocity we refer the reader to the next section (Section **??**) and for the presentation of the Brandes' study to Section **??**.

Some meaningful examples of this study are shown in Figure 2.2 and Figure 2.3. The top two figures represent curves obtained with fixed values of the first shape parameter (Φ), while the second shape parameter ($d_\mathrm{n}/d_\mathrm{v}$ and $\Phi_\perp$, respectively) is left free. The *colorbar* on the right represents the value assumed by the free parameter. The range of values chosen and their discretization is the same for both models. We can observe an opposite behaviour of the obtained curves w.r.t. their second parameter, and, furthermore, that the Ganser model is more sensitive to a

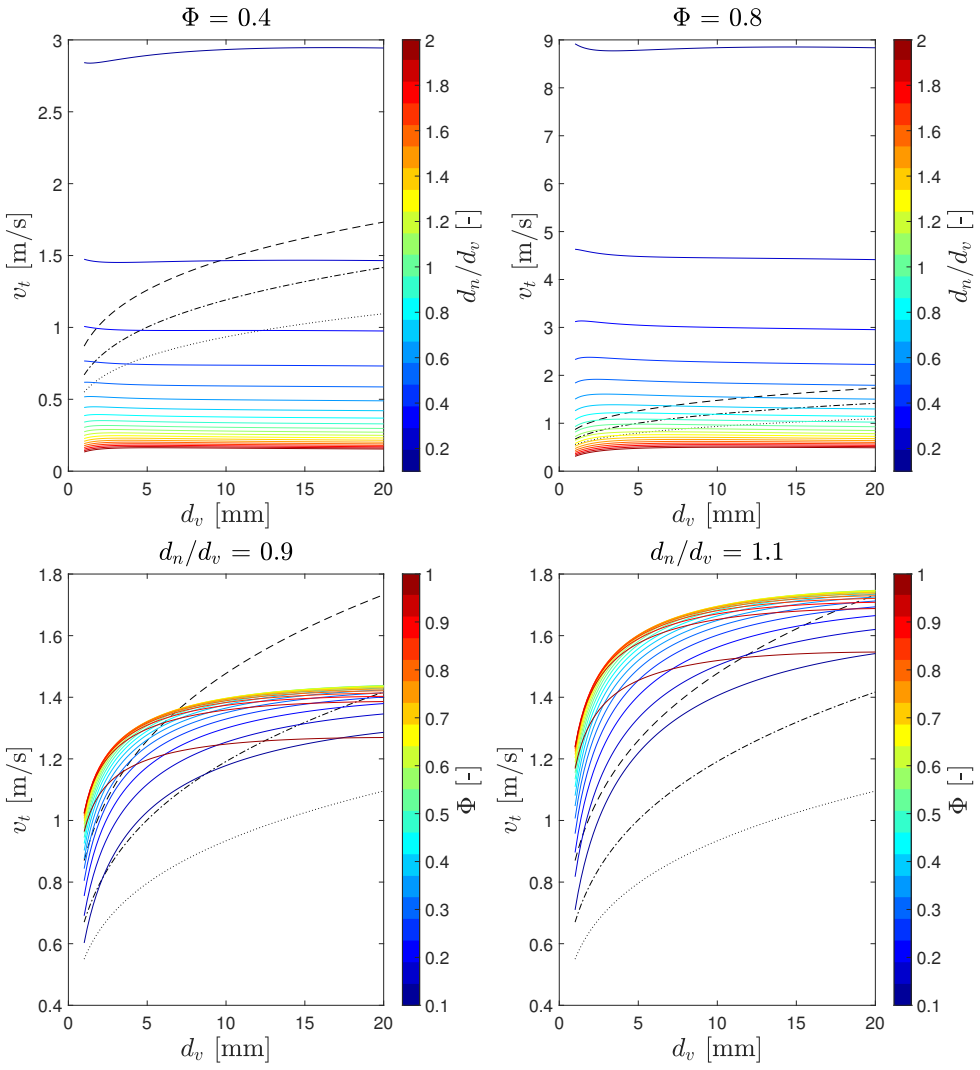

Figure 2.2: Sensitivity study of the Ganser model. Black lines are experimental curves from [**BrandesIkedEtAl-2008**], representing the mean terminal velocity of snowflakes during snowfalls of different temperatures: - - - −1 °C, -·-· −5 °C, ····· −10 °C

change in the ratio $\frac{d_\mathrm{n}}{d_\mathrm{v}}$ than the model by Höltzer and Sommerfeld to a change in $\Phi_\perp$. This appears clear recalling that $\Phi_\perp \approx (\frac{d_\mathrm{v}}{d_\mathrm{n}})^2$. Looking at the bottom figures, instead, we can observe a very similar behaviour of the two models w.r.t. a change in the sphericity.

Both models appear to be a viable choice for the inference of the shape descriptors. We select the model by Höltzer and Sommerfeld arbitrarily, keeping in mind that its lesser sensitivity on $\Phi_\perp$ will be helpful, as a minor precision on the inferred value of that parameter will be required.

This choice is also supported by the recent study of the European project ICE GENESIS can I cite them?, which experimentally confirmed that the Höltzer and Sommerfeld model is the most appropriate for the description of snowflakes.

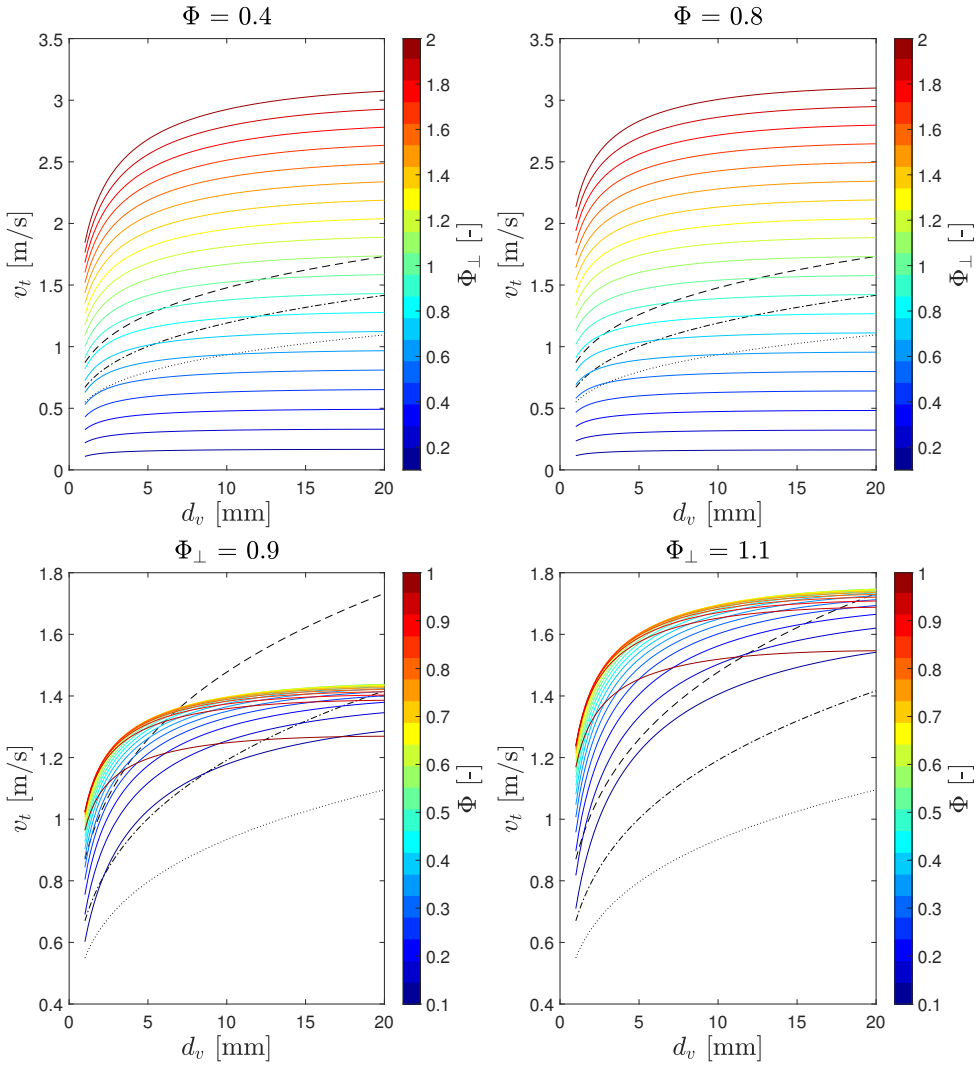

Figure 2.3: Sensitivity study of the Höltzer and Sommerfeld model. Black lines are experimental curves from **[BrandesIkedEtAl-2008]**, representing the mean terminal velocity of snowflakes during snowfalls of different temperatures: - - - −1 °C, - · - −5 °C, ····· −10 °C

Chapter 3

Parameter Estimation

3.1 Problem Formulation

Variables, unknown, data declaration.

3.2 Bayes Theorem

Theoretical background on Data Analysis using the Bayes approach. Choice of the prior and the likelihood to find the single, best parameter that explains a certain data set.

3.3 Gaussian Mixture Model

Need of a multi-modal distribution of the parameter: in a cloud more that one type of shape can be present. Modification of the Likelihood function using GMMs.

3.4 Numerical Implementation

General scheme of the program: Iteratively increase the number of mode allowed up to a certain convergence criterion (Da vedere con Giulio)

3.4.1 Maximization of the Posterior/Likelihood

Calculation of a single posterior element

- brute force algorithm
- optimization (Genetic Algorithm)
- Markov-chain method (?)

Chapter 4

Results

In this chapter the main results obtained using the procedure and the code proposed in Chapter 3 will be analyzed and discussed. The results are divided in three different test cases. The first provides a verification of the code: a totally artificial dataset is generated to ensure that the program is capable of retrieving the correct information *hidden* in the dataset. In the second test case the code will be applied to data coming from experimental measurements, although, as will be explained in Section 4.2.1 and Section 4.2.2, it is only possible to use a reconstruction of the real dataset, as the raw measurements are not available.

4.1 Test case 1 - Code Verification

In this first test case the goal is to verify that the procedure described in Chapter 3 can correctly infer the parameter distribution present in a given dataset. The results provided cannot be related to a real cloud composition.

The synthetic data set is generated starting from an arbitrarily chosen distribution of shape parameters. For simplicity, we will start considering only one parameter, namely ψ. The distribution of ψ is a bimodal Gaussian Mixture, with the two maxima in $\underline{\mu} = [0.3, 0.5]$ and a constant standard deviation σ_ψ of 0.01. The two modes are chosen with different mixing length: $\underline{\pi} = [0.7, 0.3]$. This distribution can represent a cloud composed at the 70% of particles with a shape descriptor ψ_1 of 0.3 and at the 30% of particles with $\psi_2 = 0.5$. The deviation of the data from their nominal value can be associated both with measurement errors, and with the natural dispersion of the particle shapes (that is a characteristic of snowflakes). The analytical expression of the distribution $N(\Psi)$ reads:

$$N(\psi) = \frac{1}{\sigma_\Psi \sqrt{2\pi}} \left(e^{-\frac{(\psi - \mu_1)^2}{2\sigma_\psi^2}} + e^{-\frac{(\psi - \mu_2)^2}{2\sigma_\psi^2}} \right) \tag{4.1}$$

This formula is sampled 200 times and the discrete distribution is showed in the histogram of Figure **??**. The generated valued are then used to create an artificial dataset, with each datum described by a volume diameter d_v, a measurement error σ, and a terminal velocity v_t, which is calculated using the corresponding value of the shape descriptor ψ. Since we are considering only one parameter, the velocity

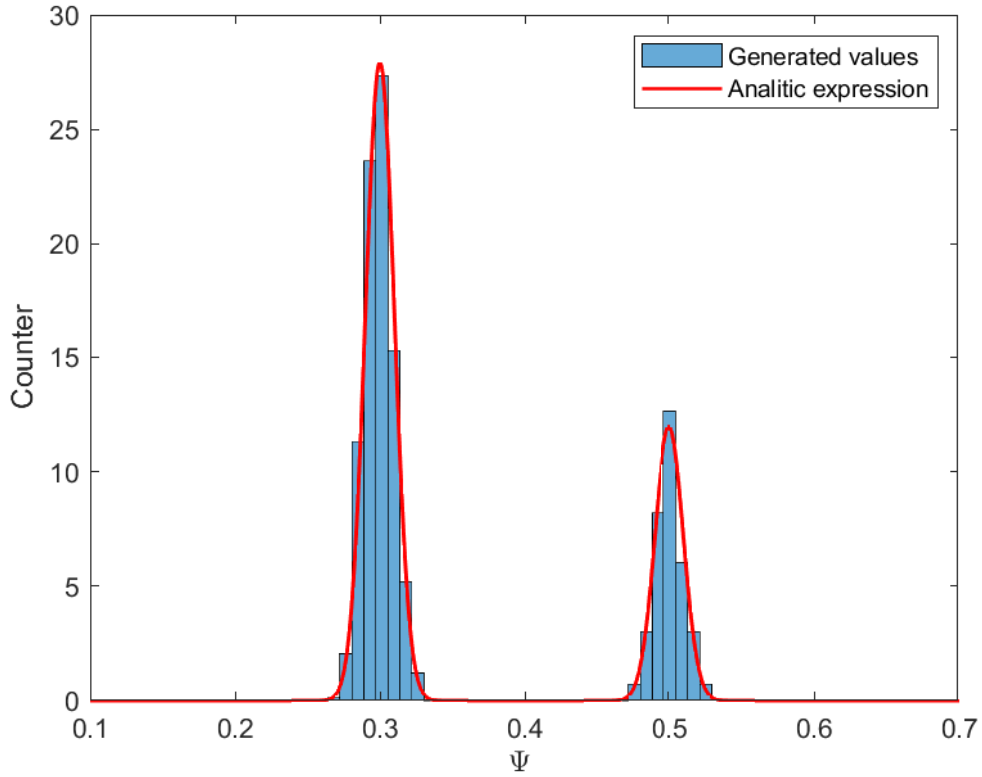

Figure 4.1: Synthetic data generated sampling a bimodal Gaussian Mixture with peaks at 0.3 and 0.5. The dataset consists in 200 values.

cannot be calculated with the model of Höltzer and Sommerfeld, and the use of an older model which depends only on one shape parameter will be meaningless. Therefore, the velocity is calculated using an arbitrary analytical formula, which, for simplicity, is:

$$v_{\mathrm{t}}(d_{\mathrm{v}}, \psi) = d_{\mathrm{v}} \cdot \psi \tag{4.2}$$

The same formula will indeed be used to calculate the terminal velocity during the parameter estimation. The diameter is also chosen arbitrarily, here random values of about 2-3mm are used.

As discussed in Section 3.4, the procedure to infer the parameter distribution is iterative. The first attempt is made allowing one single mode in the posterior (M = 1) and, since the number of parameters involved has been chosen to be small on purpose, the brute force algorithm is used. In this way the whole posterior is calculated (instead of only its maximum), and it can be graphically represented, as shown in Figure **??**. As expected the posterior has a maximum that is different from both μ_1 and μ_2. The choice of M = 1 means, as explained in Section 3.2 and 3.3, that the code infers the single, best parameter that explains all the data considered. The calculated maximum $\psi = 0.35$ is approximately the weighted average of μ_1 and μ_2, which is $0.7\mu_1 + 0.3\mu_2 = 0.36$.

The procedure requires then to increase the number of modes allowed, thus M is set to 2 and the posterior is computed again. The results are shown in Figure **??**.

The posterior has two equivalent maxima, in fact the problem is invariant to

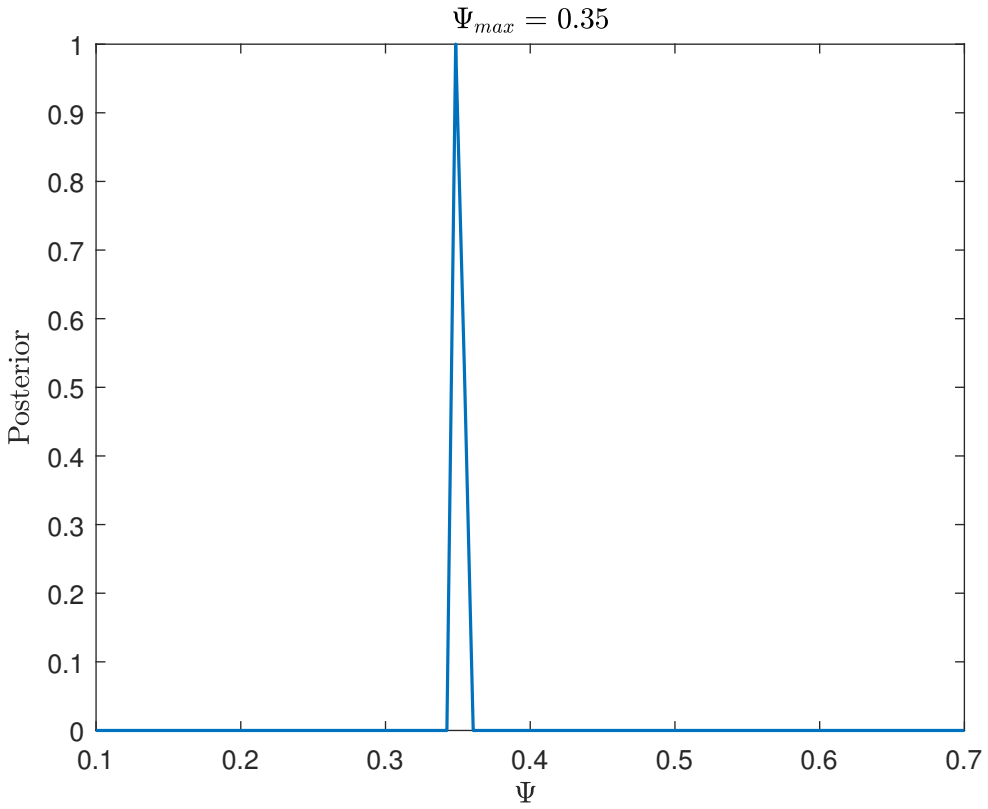

Figure 4.2

the transformation described in Equation 4.3.

$$\begin{cases} \psi_1 = \psi_2 \\ \psi_2 = \psi_1 \end{cases} \tag{4.3}$$

For the sake of completeness both the posterior are shown and explained this time, but, since the information they provide is the same, from now on, only one maximum per solution will be considered.

Being M = 2, the posterior has three independent parameters that are inferred: the maximum of the first mode ψ_1, the maximum of the second mode ψ_2 and the independent mixing length π (see Section 3.3). The two actual values of the mixing length are then reconstructed applying the constraint described in missing reference, obtaining:

$$\begin{cases} \pi_1 = \pi \\ \pi_2 = 1 - \pi \end{cases} \tag{4.4}$$

The two modes, which belong to the first maximum (denoted with the superscript 1), are $(\psi_1, \pi_1)^1 = (0.3, 0.7)$ and $(\psi_2, \pi_2)^1 = (0.5, 0.3)$, as written in the title of Figure **??**. On the figure itself are represented two curves: the first one (blue line) shows the dependency of the posterior on the first mode, with the value of the second mode and the mixing length taken as constants and corresponding to the maximum, namely $P(\psi_1) = P(\psi_1, \psi_{2,\max}, \pi_{\max})$; the second one (red line) shows the

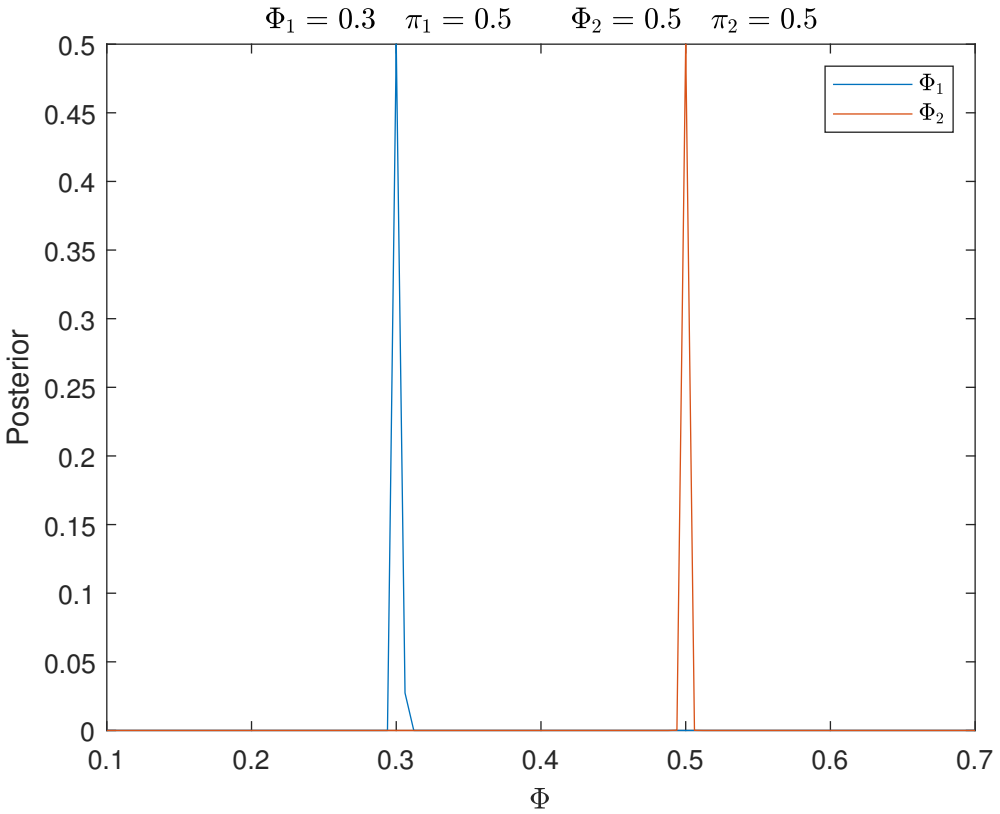

Figure 4.3

same dependency w.r.t the second mode: $P(\psi_2) = P(\psi_{1,\max}, \psi_2, \pi_{\max})$. Following the same scheme, Figure **??** shows that the second maximum contains the two modes $(\psi_1, \pi_1)^2 = (0.5, 0.3)$ and $(\psi_2, \pi_2)^2 = (0.3, 0.7)$. These are indeed the results that we were looking for, but the procedure now provides that the number of modes is increased again, and only if the solution at M = 3 coincides with the previous one (M = 2) we can exit the loop.

The posterior resulting from the third iteration of the scheme is represented in Figure **??**. instert comment

- 1 parameter (Figure 4.1, 4.2, 4.3, 4.4)
- 2 parameters (Figure 4.5, 4.6, 4.7)

4.2 Test case 2 - Experimental Dataset

Brief description of the available experimental campaigns (Brandes + other 2 references) and their limitations.

4.2.1 Brandes Experimental campaign

Description of the Brandes results and impossibility to use the raw data

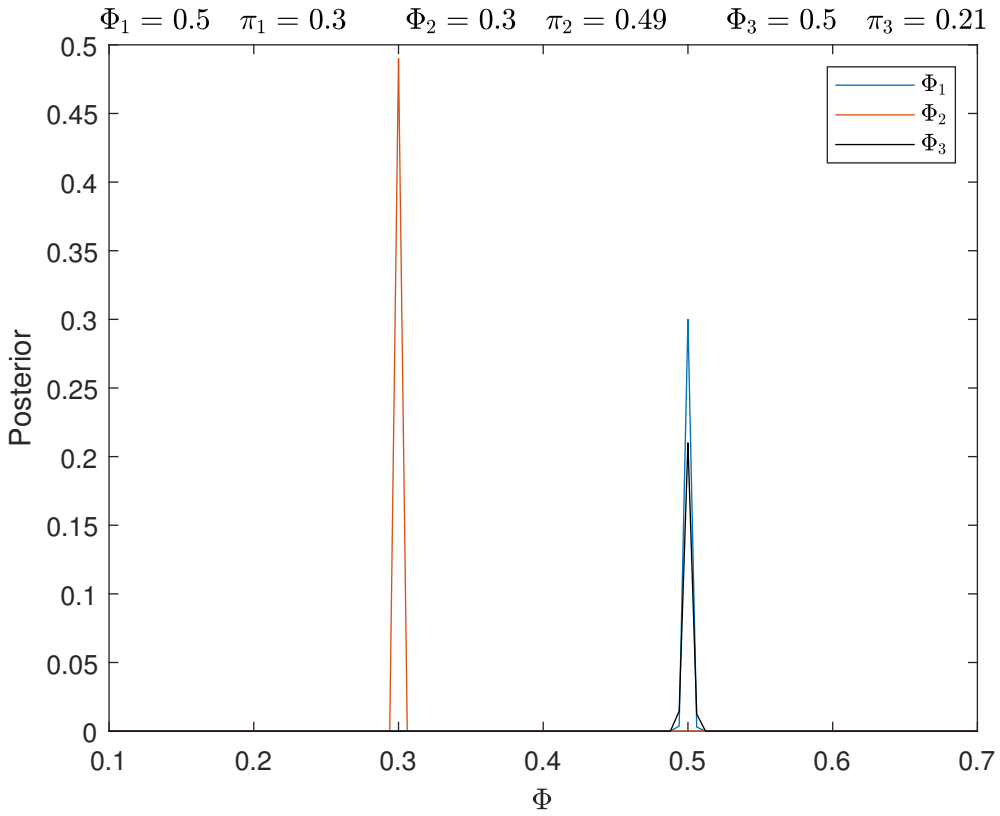

Figure 4.4

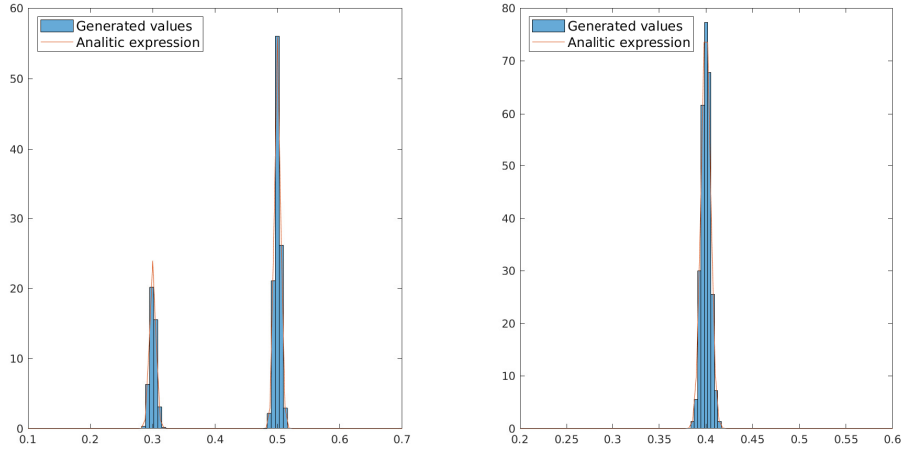

Figure 4.5

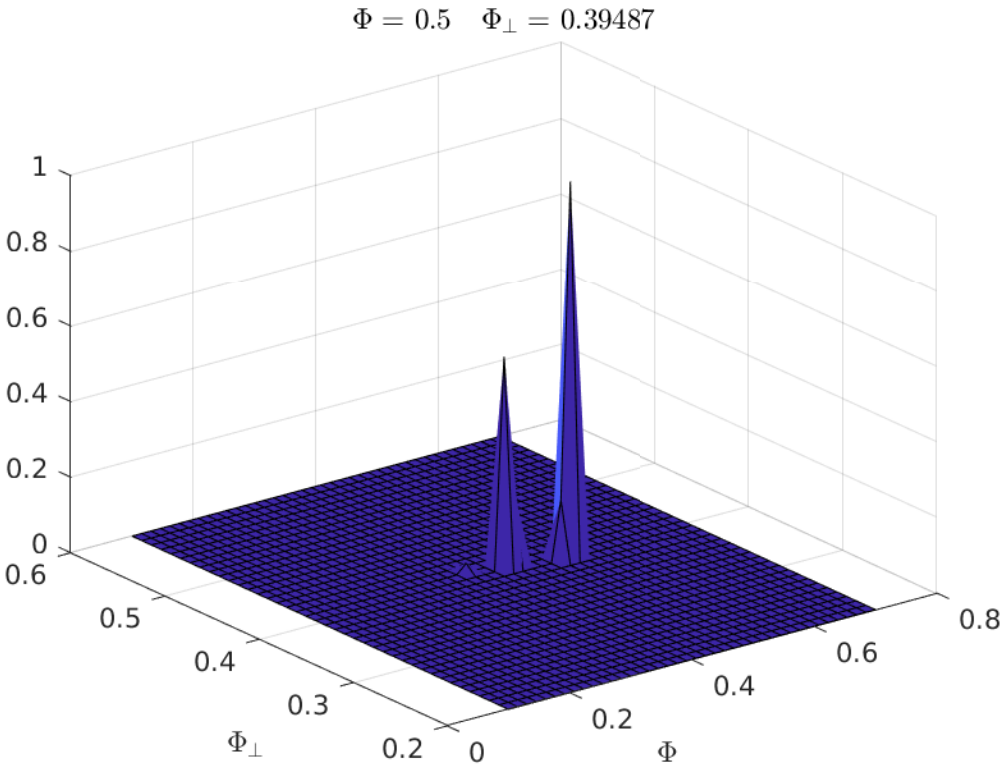

Figure 4.6

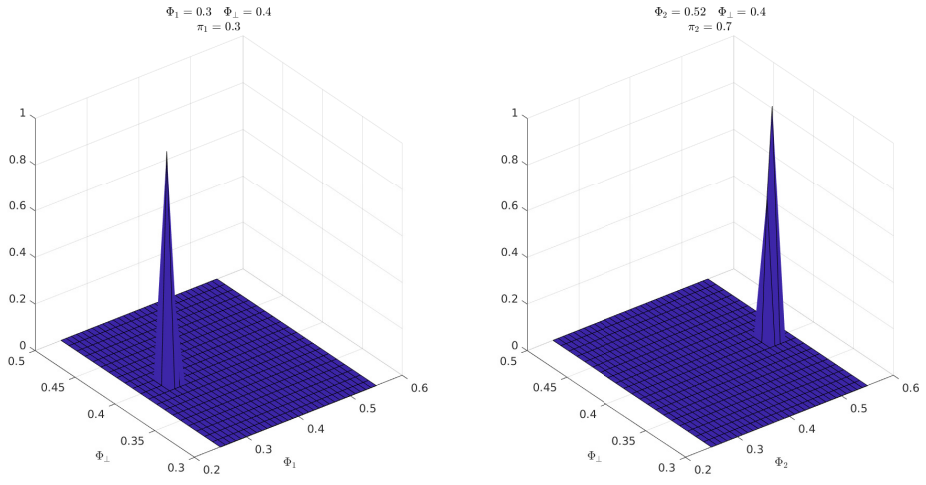

Figure 4.7

4.2.2 Data Set generation

Generation of an artificial data set starting from the relations discovered by Brandes. The dependency on the diameter distribution is not taken into account as it can be retrieved a posteriori.

4.2.3 Application to the Brandes data set

- Example for 1 diameter interval
- Shape parameters - diameter distribution (Work in progress)

4.3 Test case 3 - Let it snow!

Falling snow test case (Check the terminal velocity distribution) with PoliDrop

Chapter 5

Application to In-Flight Ice Accretion

5.1 PoliDrop

Description of PoliDrop Implementation of the chosen formula for the c_D in PoliDrop

5.2 Cloud generation

Some rules to generate the cloud by PoliDrop

5.3 Blowing snow example

Blowing snow test case: β on a profile

Chapter 6

Conclusions and Future developments